Petroleum Science 23 (2026) 2846–2862

Contents lists available at ScienceDirect

Petroleum Science

journal homepage: www.keaipublishing.com/en/journals/petroleum-science

Original Paper

Analytical model for lateral peak soil resistance based on pipe-soil interaction full-scale test and numerical simulation

Xiao-Ben Liu [a,b,*], Tian-Wei Kong [a,b], Peng-Chao Chen [c], Dong Zhang [a,b], Wei Huang [a,b], Lei Li [a,b], Rui Guo [a,b]

[a] College of Mechanical and Transportation Engineering, China University of Petroleum (Beijing), Beijing, 102249, China
[b] National Engineering Research Center for Pipeline Safety, China University of Petroleum (Beijing), Beijing, 102249, China
[c] PipeChina Institute of Science and Technology, Tianjin, 300450, China

ARTICLE INFO

Article history:
Received 26 December 2024
Received in revised form
7 July 2025
Accepted 22 December 2025
Available online 25 December 2025

Edited by Xi Zhang

Keywords:
Pipe-soil interaction
Model tests
Finite element simulation
Lateral peak soil resistance
Modified

ABSTRACT

Pipelines, as critical infrastructure for oil and gas transportation, require precise evaluation of peak loads in displacement-prone zones to ensure operational safety. The current design guidelines for lateral peak soil resistance (ALA-2001 and PRCI-2009) are based on early analytical studies with limited simulations and physical test data. These guidelines fail to adequately account for the coupled effects of soil friction and cohesion while also overlooking asymmetric soil constraints. These limitations raise significant concerns regarding their applicability in practical engineering scenarios, necessitating the development of more accurate analytical methods. The present study combines full-scale lateral pipe-soil interaction tests with finite element modeling via the coupled Eulerian-Lagrangian approach in ABAQUS/Explicit. After validation, parametric studies were conducted to establish a comprehensive database of lateral peak soil resistances. Based on the observed resistance development patterns, the lateral peak resistance calculation equation in ALA-2001 was modified to provide a more accurate analytical model capable of better reflecting real-world pipe-soil interaction behavior. The reliability of the proposed model was confirmed through independent physical tests, demonstrating its significant value for pipeline engineering design and safety assessment.

1. Introduction

As essential components of energy transport, onshore oil and gas pipelines play a crucial role in global infrastructure. With rapid economic development and the growing energy demands, countries around the world are expanding their pipeline networks (Liang et al., 2025). However, geological hazards such as seismic faults and landslides impose significant displacement loads that threaten pipeline integrity (Zhang, 2024). Therefore, it is crucial to accurately determine lateral peak soil resistance for designing pipelines in hazardous areas.

To date, pipe-soil interactions have been investigated using theoretical analysis, numerical simulation, and experimental methods. However, theoretical approach for accurate determination of the peak soil resistance in pipe-soil interactions does not currently exist. Therefore, model tests and numerical analysis have become the primary strategies for studying pipe-soil interactions.

Hansen and Brinch (1961) developed an analytical model for determining lateral force-bearing capacity of rigid piles, introducing soil pressure coefficients that were widely adopted. Further, Christensen validated this theory through pile-soil interaction experiments using 26 wooden model piles in sand. Audibert and Nyman (1977) pioneered the experimental research on pipe-soil interaction in sandy soils. Based on their test results and Hansen's theoretical framework, they proposed a methodology for calculating the peak soil resistance under horizontal pipeline loading. Trautmann and O'Rourke conducted experimental research on pipe-soil interaction in sandy soils, deriving load-

* Corresponding author.
E-mail address: xiaobenliu@cup.edu.cn (X.-B. Liu).
Peer review under the responsibility of China University of Petroleum (Beijing).

https://doi.org/10.1016/j.petsci.2025.12.035

displacement curves for various burial depths and pipe diameters. Their bilinear simplification of nonlinear curves was later incorporated in industry standards. Building on this foundation, they adapted Ovesen's anchor plate model to estimate the lateral peak soil resistances for pipes in sandy soils. Notably, Hansen's horizontal bearing coefficients were 50%–100% higher than Ovesen's (Ovesen and Bulletin, 1964; Trautmann and O'Rourke, 1985). Wantland et al. (1982) extended this research to clay soils, using limit analysis to derive peak soil resistance equations for rectangular foundations. The findings were incorporated into ASCE's (1984) seismic design guidelines for oil and gas pipeline systems, providing distinct equations for sand and clay. Subsequent research has focused on refining predictive equations. Hsu et al. studied pipe-soil interaction and investigated the impact of sand density and burial depth, demonstrating that the horizontal load-bearing coefficient was within the range of predictions made by using Hansen's and Ovesen's models (Hsu, 1996; Hsu et al., 2001, 2006). ALA's (2001) buried steel pipe design guidelines consolidated ASCE's research, introducing unified equations for peak soil resistance in both sandy and clayey soils by using Hansen's coefficient. This equation has been widely adopted, appearing in PRCI's (2009) natural gas pipeline seismic guidelines (2004) and China's seismic technical code for oil and gas transmission pipeline engineering (GB/T 50470-2017) (MOHURD, 2017).

Owing to advancements in computing technology, finite element (FE) simulation techniques have become prevalent among researchers studying pipe-soil interaction. After Yimsiri conducted FE analysis of pipe-soil interaction in sand, PRCI developed schematic designs for horizontal load-bearing coefficients for deeply buried pipelines and incorporated recommendations on clay relationships from C-CORE (C-CORE, 2003; Yimsiri et al., 2004). These adjustments were reflected in the guidelines for the seismic design and assessment of natural gas and liquid hydrocarbon pipelines (2009), while the computational form of the equations remained unchanged. Guo and Stolle (2005) conducted a numerical study on the effects of sand, and thus revised the horizontal load-bearing coefficient equations for sandy soils. However, its scope is limited as the analysis was conducted exclusively on sandy soils. Kouretzis et al. (2013) used large-deformation FE method (FEM) to model trench-backfilled pipes in loose sand, finding lateral resistance insensitive to friction angle variations, leading to a new sand-specific coefficient calculation method.

Accordingly, the equations commonly employed in standards and design guidelines for calculating lateral peak soil resistance in pipe-soil interaction originate from early theoretical studies, tests, and numerical simulations with limited variations in soil properties. Many scholars have not effectively considered the combined effects of cohesion and friction, which presents significant applicability issues when these analytical equations are utilized to calculate resistance for various soil types. Furthermore, these analytical solutions fail to account for pipeline uplift phenomena caused by asymmetric soil constraints. To address these limitations, in this study, full-scale pipe-soil interaction tests were conducted on diverse soil types. Following experimental validation, an FE numerical simulation model was developed via the coupled Eulerian–Lagrangian (CEL) method in ABAQUS/Explicit, which demonstrated relatively good capability in characterizing pipe-soil interactions under large deformation conditions. Numerical simulation analyses were conducted to establish a database of lateral peak soil resistance covering 180 typical working conditions (6 soil types $\times$ 5 burial depths $\times$ 6 pipe diameters). The study not only systematically evaluated the applicability of the ALA-2001 and PRCI-2009, but also enhanced the numerical accuracy of these existing specifications (ALA-2001/PRCI-2009) in calculating lateral peak soil resistance under asymmetric constraint conditions while also considering the coupled friction-cohesion effect. The proposed equation was further validated through comparative analysis with physical test results reported by other researchers, with particular emphasis on performance variations among different analytical equations under specific working conditions. Fig. 1 (technical route) illustrates that the present study involved expensive pipe-soil interaction tests and relatively extensive numerical simulations, which significantly improved existing methods for calculating lateral peak soil resistance. The refined methodology provides more reliable predictive tools for practical pipeline engineering applications, in particular, for addressing previously insufficient characterization of soil behavior in existing research.

2. Full-scale pipe–soil interaction test

2.1. Test apparatus and procedure

To investigate the complete evolution process of soil resistance in lateral pipe-soil interaction and provide authentic, verifiable experimental data for numerical simulation models, a specialized lateral pipe-soil interaction test apparatus was designed and constructed. Through FE simulation analysis and verification, the internal dimensions of the test apparatus were determined as length $\times$ width $\times$ height: 3504 mm $\times$ 1000 mm $\times$ 1650 mm, ensuring sufficient elimination of boundary effects (Fig. 2). The box structure, integrated with an external steel frame, ensured the strength and stability of the apparatus. The bottom plate and two side covers were crafted from steel plates. Horizontal sliding grooves, each 100 mm wide, were installed on both sides of the box to constrain the longitudinal displacement of the pipeline during testing. Soil retaining plates were mounted on the inner sides of the box to prevent soil from escaping through the sliding grooves during pipeline movement. These plates moved simultaneously with the pipeline. The pipes with diameters of 90 and 219 mm were used in the tests and were made of X65 steel.

The experiment primarily investigated the soil-induced loads acting on the pipeline while intentionally disregarding the pipe's own deformation. Consequently, solid steel columns and thick-walled pipes were employed to ensure structural stability. A solid steel column with a diameter of 90 mm and a length of 1400 mm was selected for the smaller pipeline. For the larger pipeline, pipe with a diameter of 219 mm, a wall thickness of 10 mm, and a length of 1000 mm was used, and a solid steel column of 90 mm diameter was inserted to serve as a driver. A hollow steel column (100 mm long) was used for fixation and connection, with joints welded to ensure structural integrity. A hydraulic cylinder, which served as the loading device, was affixed to the side panel of box. A spoked pressure sensor mounted at the front end of the piston rod was used to measure the load, whereas a wire-type displacement sensor was utilized to record displacement. At the onset of the experiment, commands were issued from a computer system to the electrical drive system to activate the servo-hydraulic power unit, which in turn drove the hydraulic cylinder for loading and unloading, thus moving the pipeline.

After filling with test soil, it was ensured that the wire-type displacement sensor and the force sensor were connected to the computer system, with all data cables loosely arranged. A camera was mounted to capture and document the testing process. The experiment was conducted in two modes: with and without the pipe. The data acquisition instruments were calibrated, and their accuracy was verified before the data acquisition and loading systems were initiated. During testing, data on the total force during loading and additional friction forces were collected. Existing literature indicates that typical loading rates for pipe-soil interaction tests range from 0.168 to 150 mm/min (Karimian,

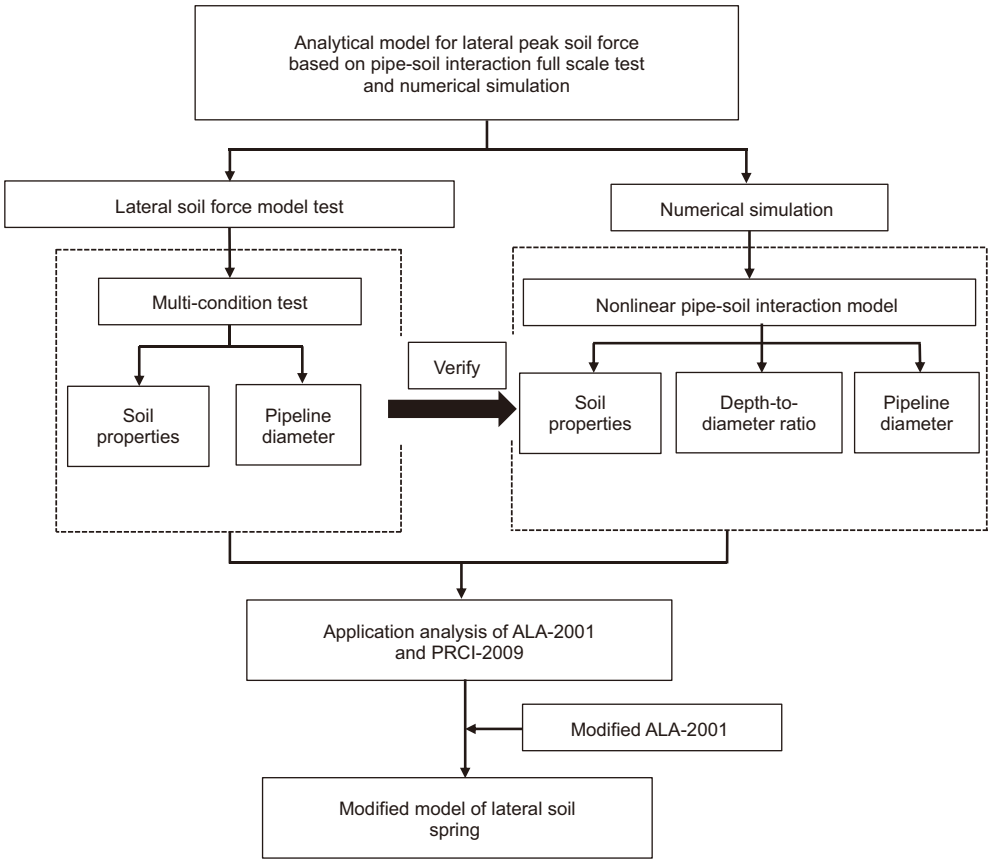

Fig. 1. Technical route.

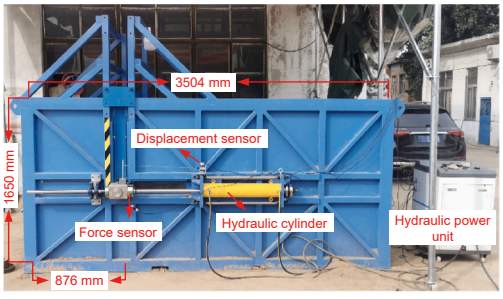

(a) External diagram of the apparatus

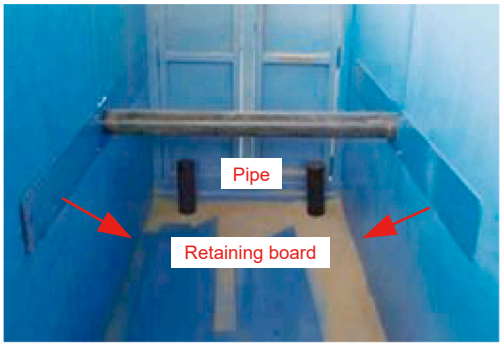

(b) Internal diagram of the apparatus

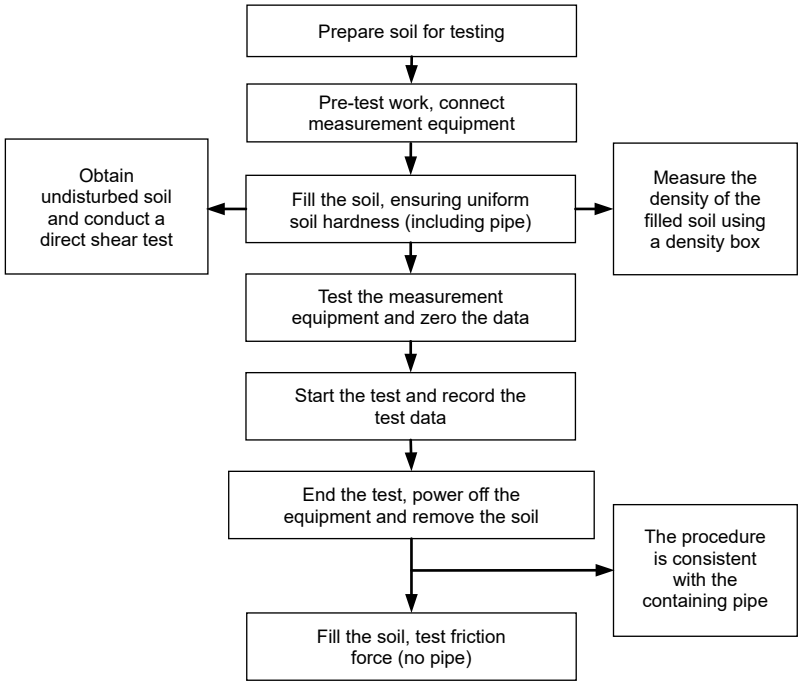

(c) Test process

Fig. 2. Test apparatus diagram and test process.

2006; Almahakeri et al., 2014; Wu et al., 2020; Ansari et al., 2021; Yue et al., 2021). Pipe loading rate was selected as 5 mm/min to maintain a quasi-static process. The data acquisition system collected data at a frequency of 1 Hz. The outlined steps were followed to conduct the tests and record the data. After each test for pipe resistance, the soil was refilled as necessary, and the friction force tests were commenced. The experimental procedure is presented in Fig. 2.

2.2. Soil parameters

Experimental-grade silty clay and sandy soils were prepared and loaded into the test chamber from the top using a winch. A stratified compaction approach was adopted for filling the clay. A soil hardness tester was used to gauge the soil hardness at various points within the same chamber layer, maintaining soil hardness between 2300 and 2500 kPa to ensure uniformity across the sample. These conditions simulated soil at a depth of approximately 1 m (Liu et al., 2019). Noteworthy, this hardness parameter specifically characterizes the soil's resistance to localized compression or penetration, and does not represent shear strength properties. For sand, the hoist's height was adjusted, allowing the soil to descend from approximately 1.6 m above the underlying soil layer. The hardness from natural deposition typically ranges from 600 to 700 kPa. Notably, the tests specifically address onshore pipeline conditions, as the testing environment for offshore pipelines differs significantly from that of onshore pipelines.

The soil samples were collected in accordance with the direct shear test procedures specified in standard for geotechnical testing method (GB/T 50123-2019) (MOHURD, 2019). To obtain undisturbed soil parameters, both cohesive and sandy soils used in this study had a certain level of cohesion that allowed them to maintain a stable morphology for testing. Therefore, all samples were prepared following the cohesive soil specimen preparation requirements stipulated in the standard. Noteworthy, the cohesion of sandy soils primarily results from capillary forces induced by moisture content. However, under constant moisture content conditions, this does not affect the measurement results of soil strength parameters. Using a ring soil sampler, standard-compliant specimens were collected. The inner surface of the ring sampler was evenly coated with Vaseline. The ring sampler was vertically inserted by applying downward pressure on its cap until the top edge was slightly below the soil surface. The sampler and its contained soil core were carefully excavated using a geotechnical spatula. Both ends of the soil specimen were then precisely trimmed flush with the sampler edges using the spatula. Finally, the specimen was hermetically sealed with plastic film to maintain constant moisture content. Direct shear tests under undrained conditions were subsequently conducted to determine the cohesion and internal friction angle. The internal friction angle for sand was 32.6° with a cohesion of 1.1 kPa, whereas for clay, it was 31.6° with a cohesion of 9.7 kPa. Soil density was measured using a density box, and parallel tests were conducted to derive the arithmetic mean. Results indicate a density of 1466 kg/m^3 for sand and 1691 kg/m^3 for clay, and Table 1 details soil parameters. Parameters not directly measured in the experiments, such as elastic modulus and Poisson's ratio, were assigned empirical values (Hua and Zheng, 2018).

2.3. Test results and analysis

(1) Sand

The testing involved four sets of tests utilizing two pipe diameters, 90 and 219 mm, with two different types of soils. The burial depth of the pipe's center (H) was 1.5 times the pipe diameter (1.5D). The following are the test results for sand. The total measured load comprises two components: the load acting on the pipe itself and the additional frictional loads from accessories. These components include retaining boards and pulleys, where friction induced by the retaining plates and the interaction between pulleys and guide rails may adversely affect measurement accuracy. Therefore, to ensure accuracy, it is necessary to eliminate this friction. The true load acting on the pipeline can be obtained by subtracting the frictional load from the total load. The proportion of frictional load in the total load gradually diminishes and gets stabilized with increased horizontal displacement. For the 90 mm diameter pipeline, the frictional load proportion decreases from an initial 34% and stabilizes at approximately 30% (see Fig. 3(a)). Similarly, for the pipeline with diameter of 219 mm, the frictional load proportion decreases from an initial 17% and stabilizes at around 15% (see Fig. 4(a)). Regarding friction, the difference between the pulley and the chute shows lesser values difference between the two cases, with the primary variance arising from the sliding friction between the retaining plate and the inner wall of the box and the soil. This indicates that during the shearing phase, the development rate of interaction forces between the pipeline and the soil is marginally slower than the friction caused by the retaining board. In the initial stages of interaction between the pipe and the soil, the reactive force exerted by the soil on the pipe is dominated by the elastic phase. The constraining force acting on the pipeline increases almost linearly as the soil particles inside reorganize and compress relatively tightly to accommodate the displacement variations in pipeline. Subsequently, the load-displacement curve becomes more gradual. This is attributed to the low cohesion and loose nature of the sand. During the displacement of the pipe, the soil compactness at the front of the pipeline movement direction changes slightly. For the pipeline with diameter of 219 mm, the slow initial increase in soil reaction force before reaching a displacement of 200 mm can be due to the non-uniformity of the soil surrounding the pipe, which is caused by improper soil filling. The soil density is lower, and the porosity is higher near the pipe, causing the soil to gradually increase its reaction force as it experiences compression from the pipe.

When the lateral peak soil resistance calculation equations provided in ALA-2001 and PRCI-2009 are used to calculate the peak soil resistance corresponding to the test conditions, as shown in Eq. (1), discrepancies arise in parameters of the horizontal bearing capacity factor for clay N_{ch} and the horizontal bearing capacity factors for sand N_{qh} in the two criteria. The percentage

Table 1
Soil parameters.

Soil	Elastic modulus, MPa	Poisson's ratio	Density, kg/m^3	Internal friction angle, °	Cohesion, kPa	Dilation angle, °
Clay	15	0.4	1691	31.6	9.7	1.6
Sand	25	0.3	1466	32.6	1.1	2.6

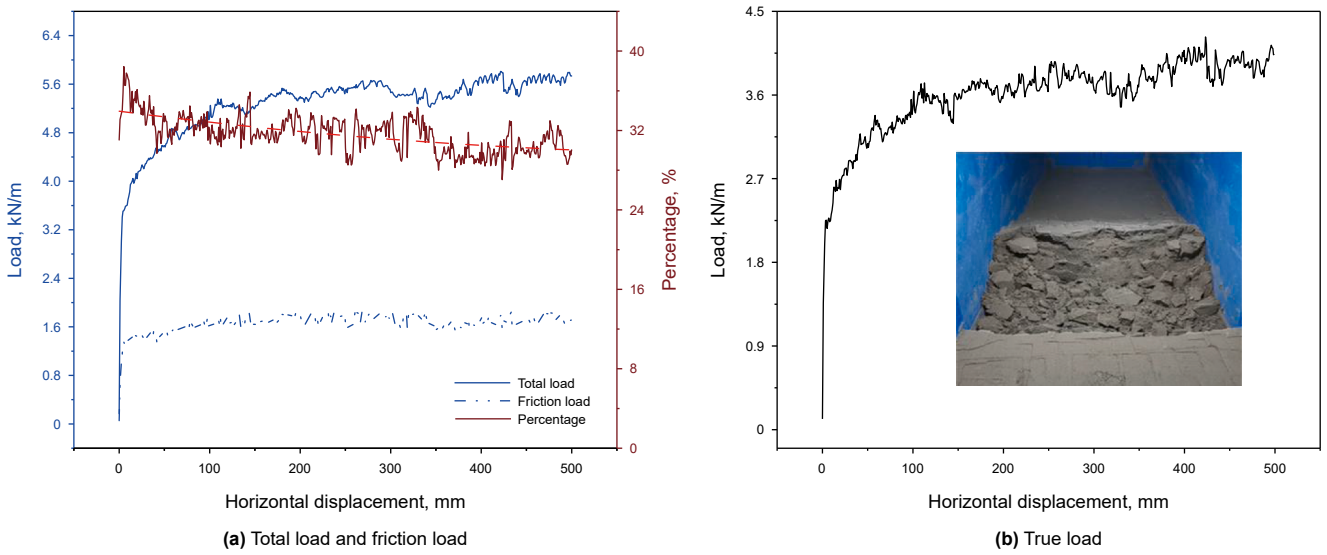

Fig. 3. Load-displacement curve graph (90 mm diameter pipeline).

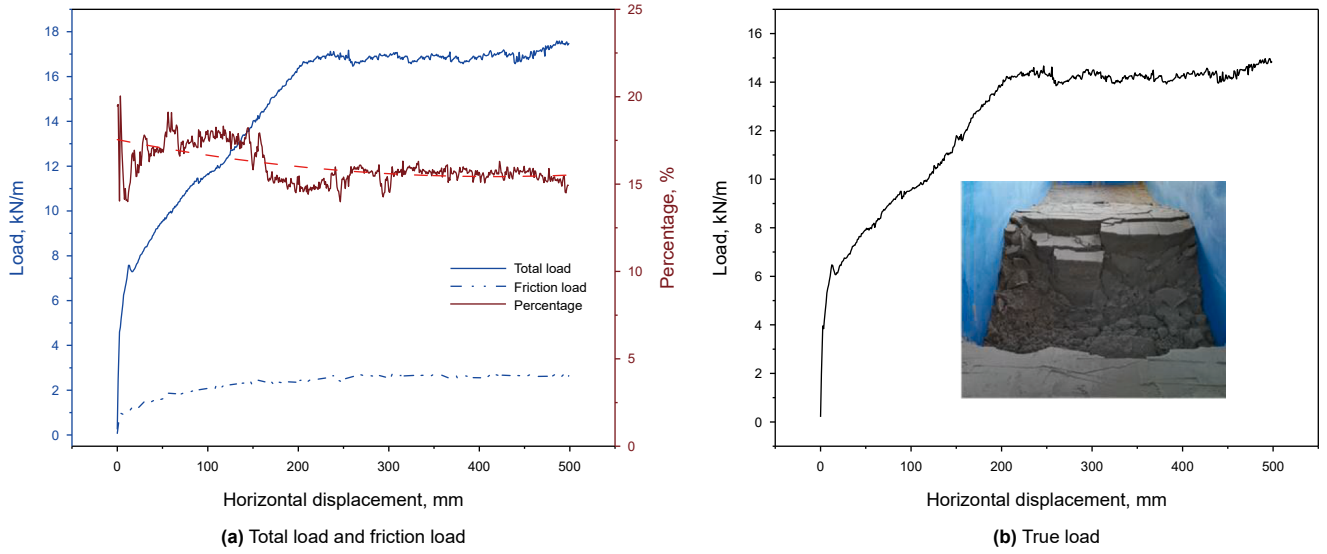

Fig. 4. Load-displacement curve graph (219 mm diameter pipeline).

deviation represents the analytical calculation results relative to the test results, as presented in Table 2, for comparative analysis. Table 3 lists the calculated values and percentages of the total value of the cohesive force and friction force-related results. The comparison results show that both ALA-2001 and PRCI-2009 predictions tend to be non-conservative compared to the test results. Predictions from PRCI-2009 are generally lower than those from ALA-2001 but higher related to cohesion compared to ALA-2001.

$$P_u = N_{ch} cD + N_{qh} \bar{\gamma} HD \quad (1)$$

where P_u is the lateral pressure exerted by the soil surrounding the buried pipeline, N/m; N_{ch} denotes the horizontal bearing capacity factor for clay; c is the cohesive strength of the backfilled soil, Pa; D is the outer diameter of the pipeline, m; N_{qh} represents the horizontal bearing capacity factor for sand; $\bar{\gamma}$ is the unit soil effective weight, N/m^3; and H is the burial depth of the pipeline center, m.

(2) Clay

The experimental results for clay demonstrate that the soil exerts significant reaction forces on the pipe with a rapid escalation over minor displacements. Owing to compaction, the clay

Table 2
Comparison of results (sand).

Type	Peak soil resistance, kN/m	ALA-2001, kN/m	Percentage deviation (ALA-2001)	PRCI-2009, kN/m	Percentage deviation (PRCI-2009)
90 mm diameter pipeline	3.8	2.6	−31.6%	1.6	−57.9%
219 mm diameter pipeline	14.3	13.3	−7.0%	7.6	−46.9%

Table 3
Numerical values and percentages related to cohesion and friction (sand), unit: kN/m.

Type	90 mm diameter pipeline		219 mm diameter pipeline	
	Cohesion-related ($N_{ch}cD$)	Friction-related ($N_{qh}\bar{\gamma}HD$)	Cohesion-related ($N_{ch}cD$)	Friction-related ($N_{qh}\bar{\gamma}HD$)
ALA-2001	0.6 (23.1%)	2.0 (76.9%)	1.4 (10.5%)	11.9 (89.5%)
PRCI-2009	0.6 (37.5%)	1.0 (62.5%)	2.0 (26.3%)	5.6 (73.7%)

Note: The cohesion and friction parameter equations were theoretically derived from the American Lifelines Alliance guidelines (ALA, 2001).

shows high cohesion and develops a macroscopic structure resembling blocky aggregates. During pipe advancement, the soil ahead of the pipe is progressively compressed until it reaches its peak strength, followed by fragmentation. This results in cyclical fluctuations in soil reaction forces: load builds up during compression and partially releases when the soil fails. For a 90 mm diameter pipeline, the upper soil layer is thin, measuring thickness of only 90 mm, and exhibits complete damage. By contrast, for a pipeline with a diameter of 219 mm, the upper soil layer sustains partial damage. Therefore, the load fluctuations in the 219 mm diameter pipeline are less pronounced than those in the 90 mm diameter pipeline. It is thus possible to anticipate that when the pipe displacement is sufficiently large, the load-displacement curve for the clay displays approximately periodic fluctuations. Increasing the thickness of the soil layer above the pipe can mitigate these fluctuations. During displacement application, for the 90 mm diameter pipeline, frictional load accounts for approximately 16%–22.5% of the total load (see Fig. 5(a)). Frictional load constitutes 7.5%–9.3% for the 219 mm diameter pipeline during stable periods (see Fig. 6(a)). The variation in frictional load is relatively modest, with the percentage fluctuation attributable to the soil's reaction forces on the pipe.

Utilizing the lateral peak soil resistance calculation equations provided in ALA-2001 and PRCI-2009, calculations were performed for the two tests, and the comparative results are displayed in Tables 4 and 5. The comparison reveals that ALA-2001 and PRCI-2009 predictions are generally non-conservative relative to the experimental results. PRCI-2009 predicts lower values than ALA-2001, although the predictions regarding cohesion-related values are slightly higher in proportion for PRCI-2009 than for ALA-2001.

3. Finite element simulation model

3.1. Model development

A numerical simulation model of pipe-soil interaction was developed based on the nonlinear FE software ABAQUS. The pipe was modeled using discrete rigid bodies to eliminate deformation effects on result accuracy. The conventional Lagrangian mesh method proved to be inadequate for simulating large soil deformations. Therefore, in this study, an Eulerian mesh approach was employed. This approach permits material flow within the grid, thereby enabling superior simulation of soil mechanical behavior. The model was developed by using the CEL algorithm, which effectively simulated soil flow characteristics under large deformations (Ko et al., 2016), providing a viable solution for significant soil deformation problems. An Eulerian body was first established, with the region simulating soil assigned specific soil properties. The upper part, referred to as the Void, served as reserved space for soil deformation, and was essential for the CEL model (Fig. 7). Contact behavior was characterized using "All with self" in ABAQUS/Explicit, where normal contact employed hard contact, and tangential contact was simulated using penalty functions.

The upper surface of the model remained unrestricted, while the two lateral surfaces parallel to the pipe axis restricted translational movement in the *Y*-direction and all rotational movements. All other surfaces limited movement in all directions. When lateral displacement was applied to the pipe, it was free to move vertically and in the direction of displacement, thus simulating realistic pipe-soil interaction scenarios. The soil mesh was finer near the pipeline location, featuring a grid size of 0.1D (where

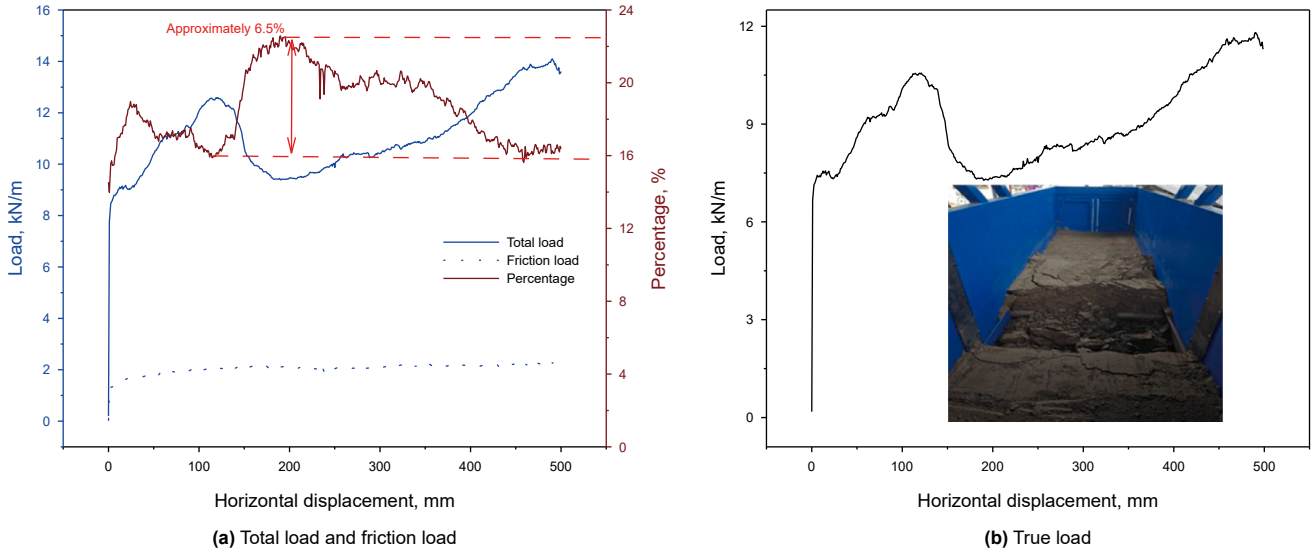

Fig. 5. Load-displacement curve graph (90 mm diameter pipeline).

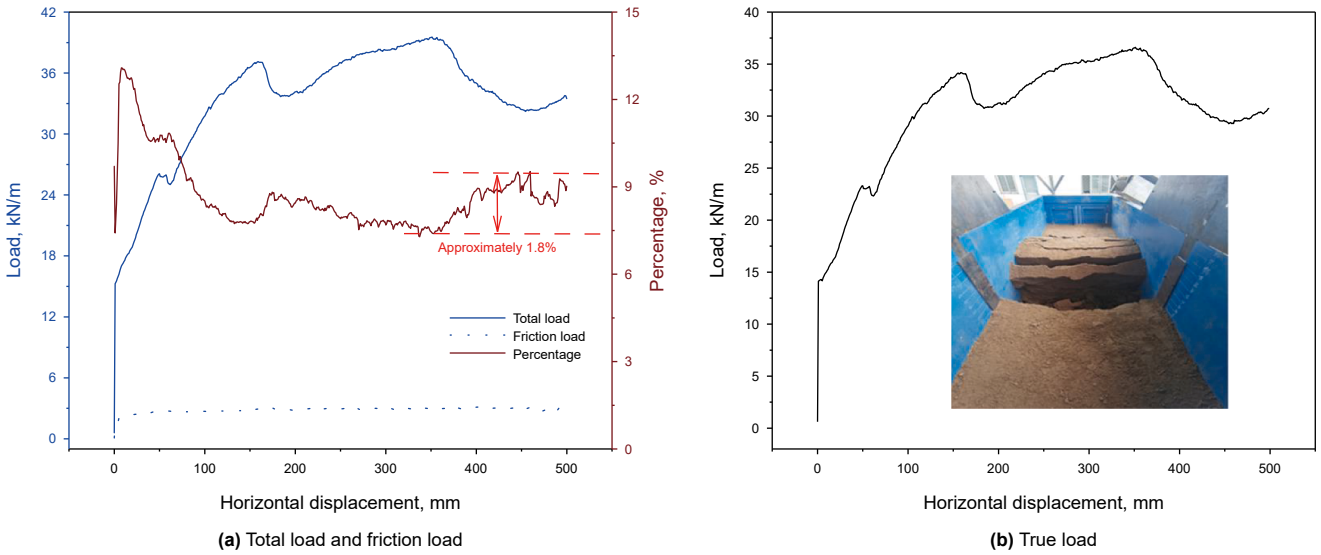

Fig. 6. Load-displacement curve graph (219 mm diameter pipeline).

Table 4
Comparison of results (Clay).

Type	Peak soil resistance, kN/m	ALA-2001, kN/m	Percentage deviation (ALA-2001)	PRCI-2009, kN/m	Percentage deviation (PRCI-2009)
90 mm diameter pipeline	9.1	7.3	−19.8%	5.4	−40.7%
219 mm diameter pipeline	32.7	25.1	−23.2%	17.5	−46.5%

Table 5
Numerical values and percentages related to cohesion and friction (Clay), unit: kN/m.

Type	90 mm diameter pipeline		219 mm diameter pipeline	
	Cohesion-related ($N_{ch}cD$)	Friction-related ($N_{qh}\bar{\gamma}HD$)	Cohesion-related ($N_{ch}cD$)	Friction-related ($N_{qh}\bar{\gamma}HD$)
ALA-2001	5.2 (71.2%)	2.1 (28.8%)	12.6 (50.2%)	12.5 (49.8%)
PRCI-2009	4.3 (79.6%)	1.1 (20.4%)	11.1 (63.4%)	6.4 (36.6%)

Note: The cohesion and friction parameter equations were theoretically derived from the American Lifelines Alliance guidelines (ALA, 2001).

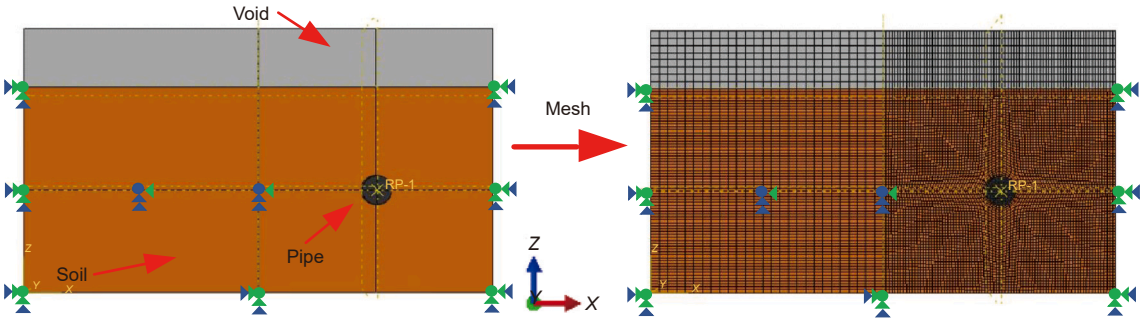

Fig. 7. Finite element model.

D represents the pipeline diameter) to ensure solution accuracy. The soil mesh became relatively coarse as it moved away from the pipeline, with a mesh size of 0.3D to enhance computational efficiency. The model included 48 circumferential grid elements around the pipeline, with an axial grid size of 0.1D (Spyros, 2021). All loads in the model were applied in two phases: initially considering the model's gravity and equilibrium; subsequently, pipeline displacement was applied.

3.2. Soil constitutive model

The Mohr–Coulomb (M–C) constitutive model is extensively utilized in geotechnical engineering (see Fig. 8). In ABAQUS, the M–C model applies a continuous smooth elliptical function, represented by Eq. (2), as the plastic potential surface. The model's yielding criterion, the shear failure criterion, is expressed by Eq. (3) (Fei and Zhang, 2013):

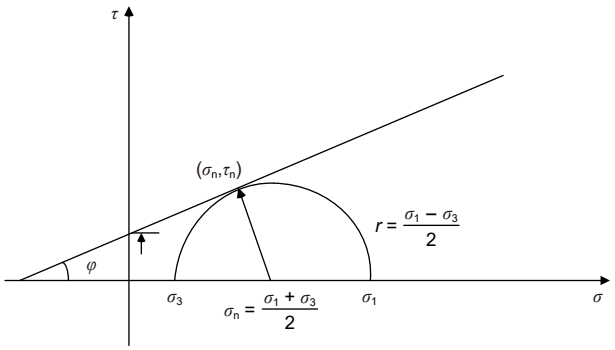

Fig. 8. Mohr–Coulomb yield criterion.

$$G=\sqrt{(\varepsilon c|_0 \tan\psi)+(R_{\mathrm{mw}}q)^2}-p\tan\psi \tag{2}$$

where ψ is the shear dilation angle, °; $c|_0$ denotes the initial cohesive strength of the material, Pa; ε is the eccentricity on the meridional plane; q–p represents the stress surface; and R_{mw} controls the shape of the function G on the plane π.

$$\tau_{\mathrm{n}}=c+\sigma_{\mathrm{n}}\tan\varphi \tag{3}$$

where τ_{n} is the shear stress on the slip plane, Pa; c denotes the cohesion of the soil, Pa; σ_{n} is the normal stress on the slip plane, Pa; and φ represents the internal friction angle of the soil, °. The Mohr circle and the M–C failure envelope under failure conditions are provided.

3.3. Accuracy verification

In this study, a finite element model was established to simulate the testing process inversely by using the abovementioned modeling approach. The comparative results are depicted in Fig. 9. For test results involving sand, the average load across the displacement range of 250–400 mm in the steady section was selected as the peak soil resistance. The average peak load following soil compaction was selected for clay as the peak soil resistance. When the pipe advanced, the soil ahead of the pipe underwent progressive compaction due to the imposed displacement, leading to continuous evolution of its mechanical properties until shear failure occurred. The M–C model is an ideal elastic-plastic model but does not accurately track soil compaction and collapse processes. As a result, for clay, the load-displacement curve lacks periodic fluctuations. Therefore, the inverse FE analysis results were used to select the average load within the stable stage region, across the displacement range of 250–400 mm, as the peak soil resistance. The comparison of peak soil resistances derived from experiments and FE inverse analysis is presented in Table 6. The maximum percentage deviation between numerical simulation results and experimental measurements was −11.4%. This deviation might have resulted from inevitable human factors during both soil compaction and soil mechanical parameter measurement processes. For instance, variations in penetrometer insertion angle and depth during soil hardness testing, as well as inherent measurement errors in soil mechanical parameter determination, are practically unavoidable in experimental procedures. The current comparative analysis results sufficiently demonstrate the high accuracy of the established FE model.

4. Numerical simulation of pipe–soil interaction

4.1. Geometric dimensions and parameters

The FE simulation model was established following the methodology described in Section 3.1. As the model dimensions vary according to different simulation conditions, the variation approach for model dimensions is specified below. When the pipe diameter is D, and the horizontal displacement (Di) is 4D, the surrounding soil extends 15D in the direction of movement, 5D behind the direction of pipeline movement, and the soil depth beneath the pipeline is 3.5D. If the pipe center depth H exceeds 3.5D, the soil depth at the pipeline's bottom is set to H. This dimensional configuration is demonstrated in simulations to mitigate the influence of boundary effects (Sarvanis et al., 2018). The upper region of the model, extending 2.5D, acts as a reserved area for soil deformation, with no observed soil spillover phenomenon during the simulation.

The soil parameters include various types of sand and clay, as referenced in “Geohazards and Pipelines” and “Engineering Geology Handbook 5th Edition” (Hua and Zheng, 2018; Spyros, 2021). Detailed values are listed in Table 7. The pipe diameters are 273, 508, 864, 1016, 1219, and 1422 mm. Pipe burial depths are 1D, 2D, 3D, 4D, and 5D, with the pipe displacement set at 4D. In total, 180 data sets were analyzed.

In simulating the lateral soil-pipe interaction at the prototype scale, the pipe's weight reflects real-world conditions, with a material density of 7800 kg/m^3. Moreover, the vertical restraint of the pipe was modeled as free, permitting vertical movement. The pipe's outer diameter and wall thickness are specified in Table 8 (MIIT, 2017).

4.2. Simulation results and analysis

Fig. 10 presents contour plots of simulated vertical displacement (VD) at various burial depths for a pipe with a diameter of 1016 mm. During lateral pipeline movement, a passive soil wedge develops in front of the pipe, resisting its advancement. At shallow burial depths, the shear failure surface of the passive zone extends to the ground surface, resulting in reduced vertical confinement and inducing an upward movement tendency of the pipeline. When lateral displacement reaches 4D (pipe diameter) under a burial depth of 1D, the pipeline ascends to the ground surface accompanied by soil rupture events. With the increase in the burial depth, the pipe experiences uplift in sand. Owing to the pronounced shear dilation effect of the sand, significant soil buildup occurs in front of the pipe. In clay, due to its higher soil cohesion, the constraint effect of the soil above the pipeline becomes more pronounced with increasing burial depth. This results in a smaller longitudinal upward displacement of the pipeline compared to sandy soil. Fig. 11 demonstrates that the pipeline uplift decreases with increasing burial depth and gradually stabilizes at around 0.75 m for sand. The uplift decreases rapidly for clay with increasing burial depth, stabilizing at approximately 0.5 m when the pipeline center depth is no less than 2D. The fundamental mechanism underlying this discrepancy originates from the increased overburden thickness with greater burial depth, which substantially enhances the self-weight and confining capacity of the soil. This enhancement necessitates overcoming increased vertical resistance during pipe uplifting. Concurrently, prolonging the failure surface propagation paths in the passive zone facilitates enhanced energy dissipation through extended soil deformation. In sandy soils, the reduced constraint

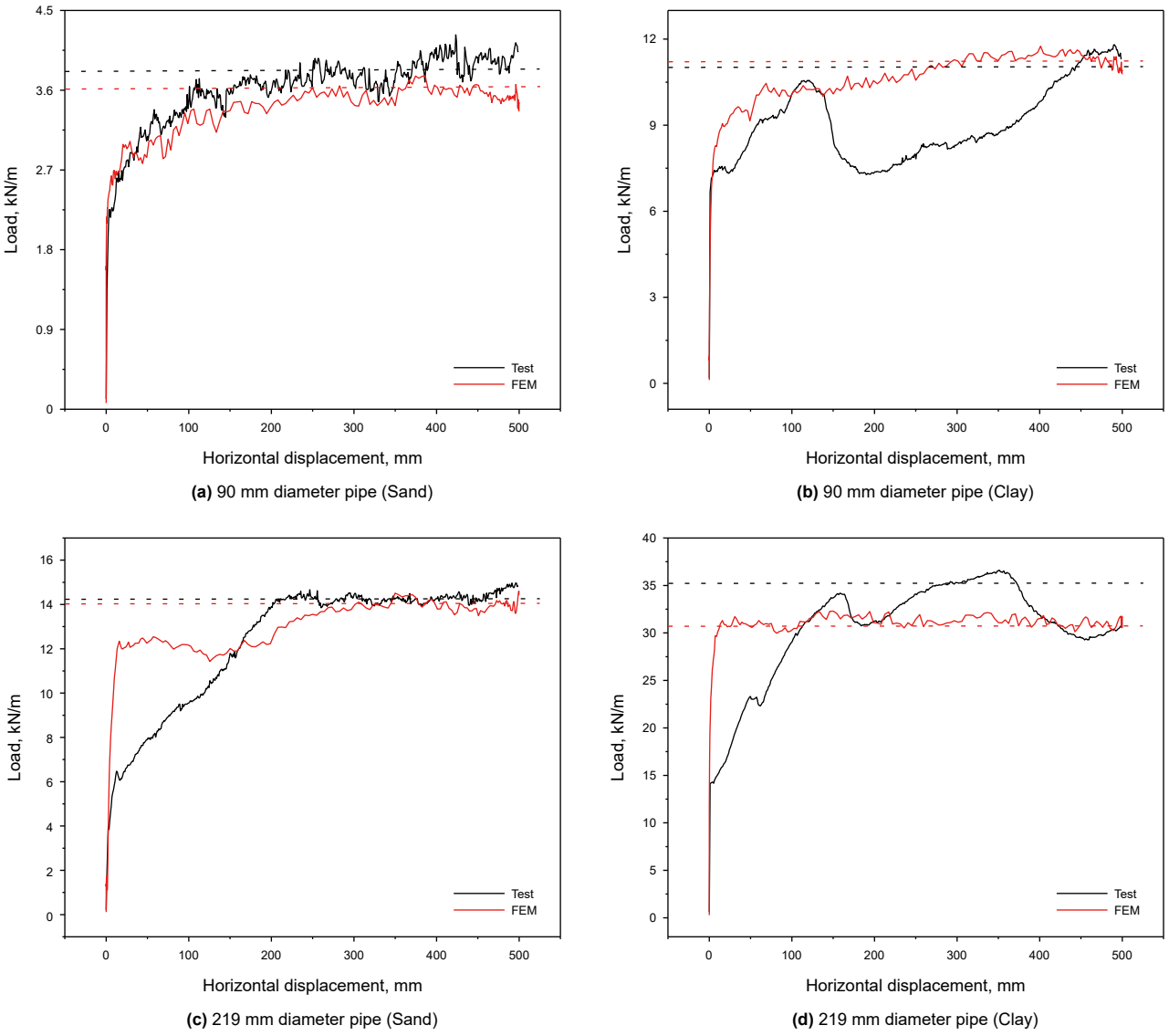

Fig. 9. Comparison of test and FEM results.

Table 6
Comparison of peak soil resistance.

Type	Test results, kN/m	Simulation results, kN/m	Percentage deviation (δ), %
90 mm diameter pipe (sand)	3.8	3.6	−5.3
90 mm diameter pipe (clay)	11.0	11.2	+1.8
219 mm diameter pipe (sand)	14.2	14.0	−1.4
219 mm diameter pipe (clay)	35.2	31.2	−11.4

Note: The percentage deviation (δ) was calculated as: ($\delta = 100\% \times (S_i - T_i)/T_i$), where S_i and T_i represent the numerical result and experimental measurement, respectively.

Table 7
Parameters for different types of soils.

Soil types	Elastic modulus, MPa	Poisson's ratio	Density, kg/m^3	Internal friction angle, °	Cohesion, kPa
Loose sand	8	0.25	1735	30	2
Medium sand	15	0.3	1837	32	3
Dense sand	35	0.35	1939	34	6
Soft clay	2	0.4	1531	22.5	40
Medium clay	7	0.4	1830	22.5	80
Stiff clay	15	0.4	2143	27.5	145

Table 8
Pipe parameter values.

Diameter, mm	Wall thickness, mm	Mass, kg/m
273	7.8	50.7
508	9.53	116.4
864	14.27	297.1
1016	17.48	427.7
1219	20.62	605.5
1422	22.23	762.5

effectiveness associated with friction dominance results in larger ultimate uplift displacements compared to cohesive soils.

Fig. 12 illustrates the load-displacement curves and VD contour plots of a model with a pipe buried at a depth of 2D and a diameter of 1016 mm in various soil types. It reveals that the peak soil resistance gradually increases for loose, medium, and dense sand. Owing to the significant uplift of the pipe at this burial depth, a noticeable attenuation occurs in the load. The contour plots on the right show that different types of sand have a seemingly negligible impact on the uplift of the pipe. Soft clay, medium clay, and stiff clay demonstrate increasing peak soil resistance. The uplift of the pipe is more pronounced in stiff clay, and due to higher soil cohesion, the decrease in load upon soil fracture becomes more significant with increasing pipeline displacement. For weak clay and medium clay, where the uplift of the pipe and soil cohesion are lower, the load does not exhibit a significant decrease when soil fracture occurs.

Fig. 13 presents load-displacement curves for pipes at a center burial depth of 2D across varying diameters. Using medium sand and medium clay as representative soils, the results indicate an overall increase in peak soil resistance with increasing pipe diameter. In medium sand, however, significant pipe uplift leads to

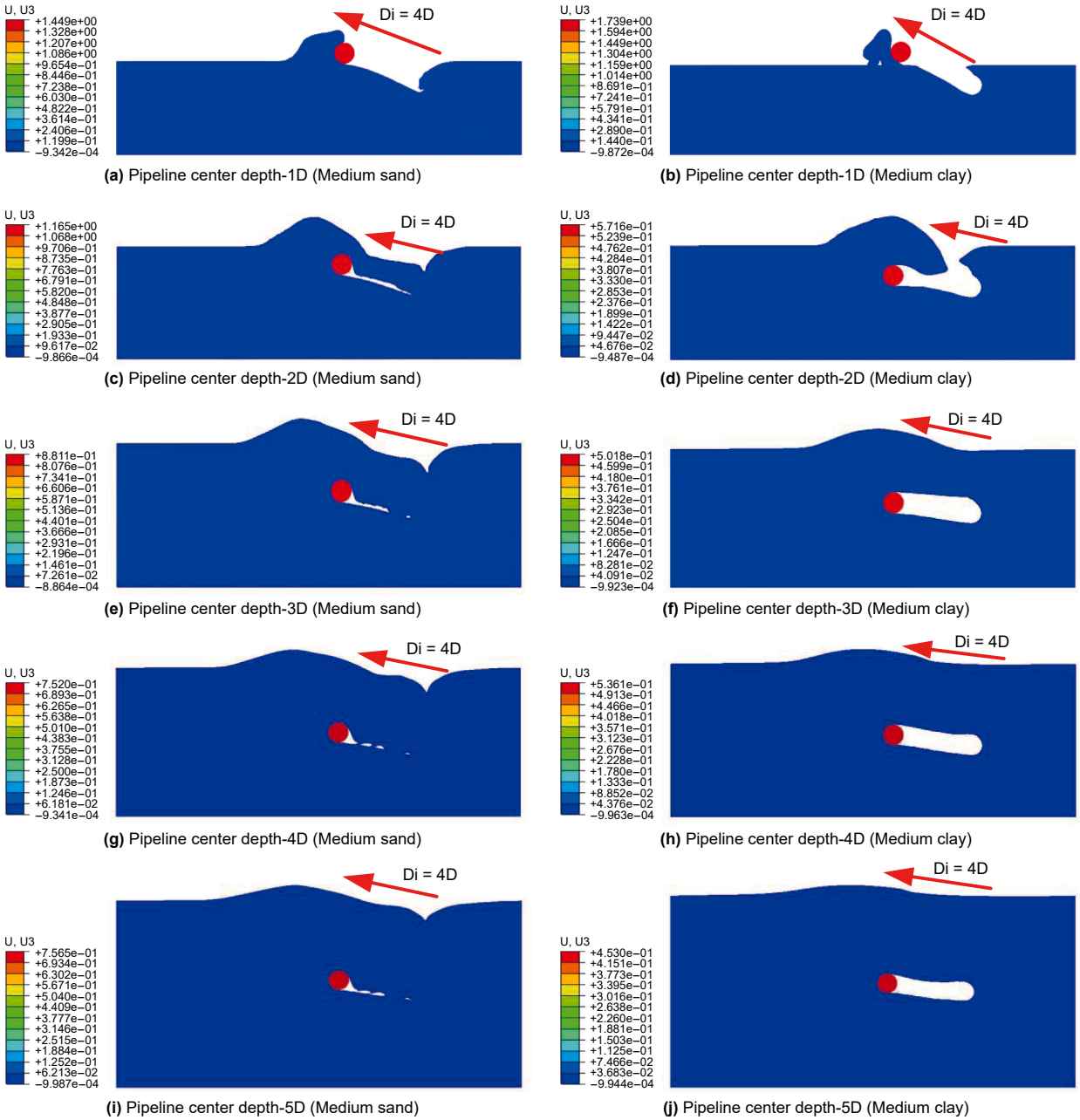

Fig. 10. Longitudinal displacements of models at various pipeline center burial depths.

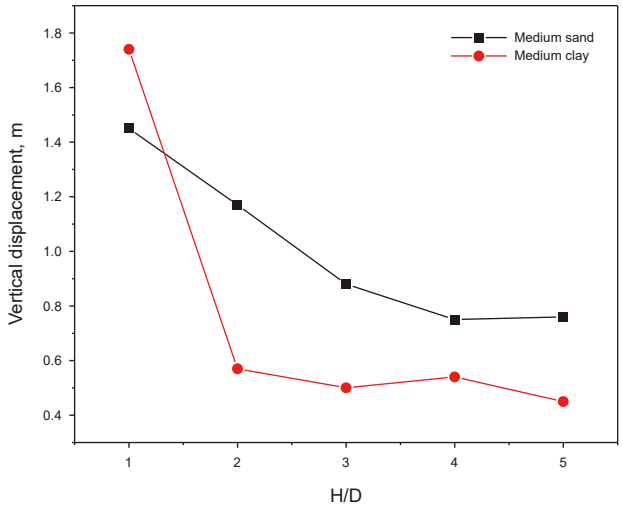

Fig. 11. Vertical displacement results of the pipe.

a marked reduction in soil load once a critical displacement threshold is reached. Conversely, for medium clay, minimal vertical pipe displacement and enhanced structural integrity of the passive zone prevent the load curve from exhibiting a distinct descending segment. During lateral pipe movement through soil, the pipe surface experiences normal stress and friction-induced tangential stress (Sarvanis et al., 2018). Fig. 14 illustrates the distribution characteristics of mechanical responses of soil during this lateral displacement. For sand, characterized by low cohesion and shear strength governed primarily by the internal friction angle, the forces exerted on the pipe stem predominantly from gravitational and frictional mechanisms. With the increase in the pipe diameter, the burial depth (2D) proportionally expands, resulting in nonlinear growth of the passive wedge volume and failure surface length in front of the pipe. Under the coupled action of normal and tangential stresses, peak soil resistance in sand demonstrates supralinear growth relative to pipe diameter (Fig. 15(a)). For soils with low cohesion, this behavior aligns with Terzaghi's passive earth pressure theory and further conforms to the phenomenon where in peak resistance in sand scales proportionally to the square of the burial depth and the bearing capacity coefficient. For clay, the high cohesion dictates the soil behavior, with the normal stress from viscous resistance being the dominant factor in the total pipe load. Although the external surface area of the pipe correlates linearly with diameter, minor contributions from soil friction introduce subtle nonlinearity. Consequently, peak soil resistance in clay exhibits a marginally supralinear increase with pipe diameter (Fig. 15(b)), consistent with the modified equation derived in this study.

Fig. 16 shows the load-displacement curves for a pipe with a diameter of 1016 mm at varying burial depths. It reveals that with the increase in the burial depth, the peak soil resistance rises due to the greater thickness of the overlying soil layers, which impose stronger constraints on the pipe. Moreover, the pipe's displacement leads to soil accumulation and upward bulging in the movement direction. These factors collectively mitigate the reduction in soil load on the pipe, resulting in a more gradual load-displacement curve. Based on previous studies and the existing equations for calculating the peak resistance of soil springs (ALA, 2001), it is acknowledged that the horizontal bearing capacity factor of a pipeline in sandy conditions exhibits a higher-order power-law relationship with the ratio of the pipe's burial depth center to its diameter (x), as demonstrated in Eq. (4). Furthermore, influenced by the relatively low cohesion of sand, the peak soil resistance in sand follows a power-law relationship with an exponent greater than one with increasing x, as demonstrated in Fig. 17(a). For clay, the relationship between the horizontal bearing capacity factor of the pipe and x is articulated in Eq. (5). As x increases, the horizontal bearing capacity factor advances at a rate less than linear. In the case of clay, the lateral load contributed by its viscous component constitutes a significant portion. Numerical simulations demonstrate that the peak soil resistance in clay follows a power-law relationship with an exponent less than one with increasing pipe diameter, as illustrated in Fig. 17(b).

The horizontal bearing capacity factor for sand is as follows:

$$N_{qh} = a + b(x) + c\left(x^2\right) + d\left(x^3\right) + e\left(x^4\right) \tag{4}$$

The horizontal bearing capacity factor for clay is as follows:

$$N_{ch} = a + b(x) + \frac{c}{(1+x)^2} + \frac{d}{(1+x)^3} \tag{5}$$

where x is the pipe centerline burial depth-to-diameter ratio; and a, b, c, d, and e are calculation-related parameters, and their values can be referenced from the American Lifelines Alliance guidelines (ALA, 2001).

4.3. Application of ALA-2001 and PRCI-2009

The vertical constraints imposed on a pipe significantly influence the peak soil resistance. Fig. 18 illustrates the comparison between the peak soil resistance and analytical results for medium sand and medium clay at various depths, considering the vertical constraint status of the pipe. The simulated pipe diameter is 1016 mm. The vertical axis on the left side of the figure indicates the peak soil resistance, while the right side depicts the percentage deviation of the results from a vertically unconstrained pipe relative to those from a vertically constrained pipe. Fig. 18 shows that with the increase in the burial depth at the center of the pipe, the differences between peak soil resistances, corresponding to whether the vertical freedom is restricted, gradually diminish. This reduction can be attributed to increased confinement caused by thicker overburden soils, during which surface effects gradually evolve into prevailing full-flow-round conditions. Moreover, owing to the stronger constraint of clay on the pipe, convergence toward consistent results occurs more rapidly with increasing burial depth. The deviation stabilizes when the burial depth reaches 4D at the pipeline center. For medium sand, ALA-2001 and PRCI-2009 provide conservative predictions when the pipe is vertically unconstrained. Conversely, the predictions necessitate case-specific discussion when the pipeline is vertically constrained. ALA-2001 and PRCI-2009 for medium clay offer non-conservative predictions when the pipe is vertically constrained, while predictions for a vertically unconstrained pipeline also require case-specific discussion.

Using the soil parameters specified in Section 4.1, lateral peak soil resistance was computed employing ALA-2001 and PRCI-2009 for varying pipe diameters and burial depths at the pipeline center. Results from FE simulations were used as a benchmark and compared with the analytical equations, with FE simulation results serving as the baseline (x-axis) for plotting. Figs. 19 and 20 demonstrate that both ALA-2001 and PRCI-2009 exhibit significant discrepancies in the calculations conducted in sand, generally overestimating the results compared to simulations; however, PRCI-2009 tends to show smaller deviations than ALA-2001. In clay, the deviations for both methods are relatively minor, generally within ±30%. This reveals the current limitations in the

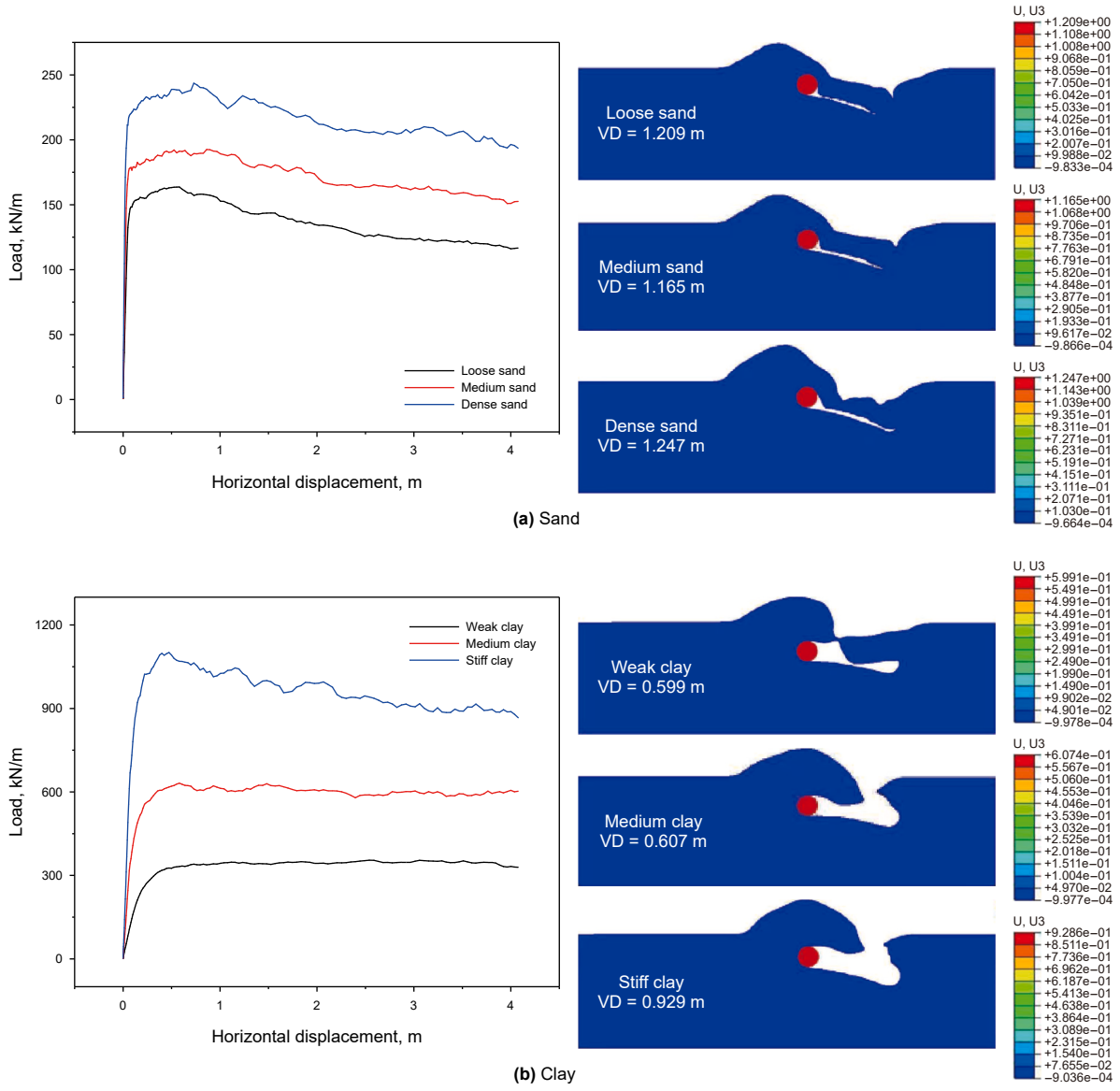

Fig. 12. Load-displacement curves and vertical displacement (VD) of the pipeline under different doil types.

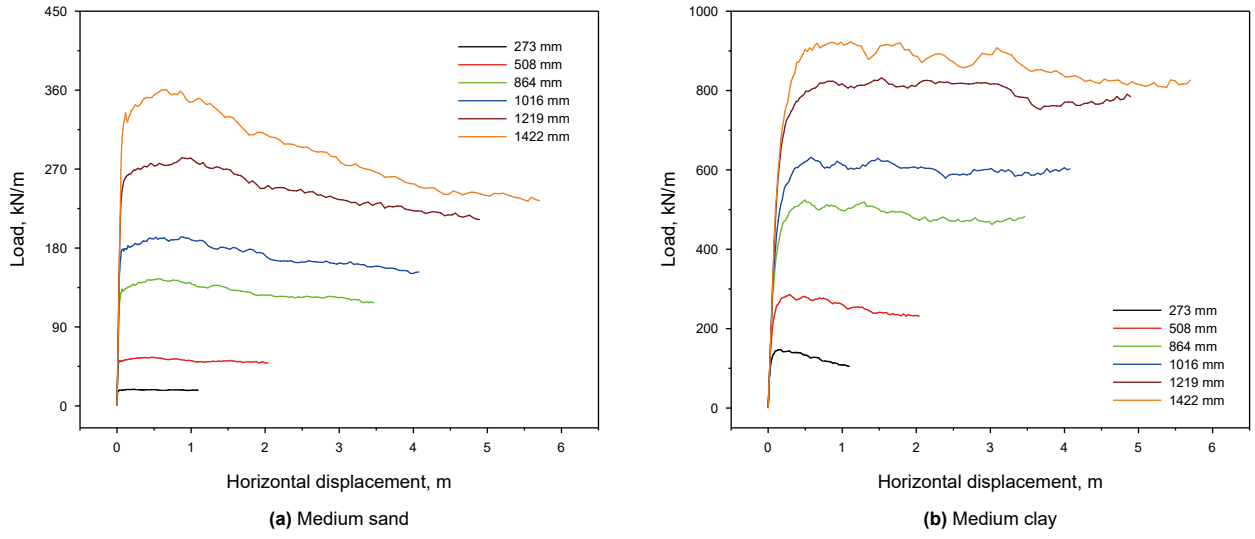

Fig. 13. Load-displacement curves under different pipe diameters.

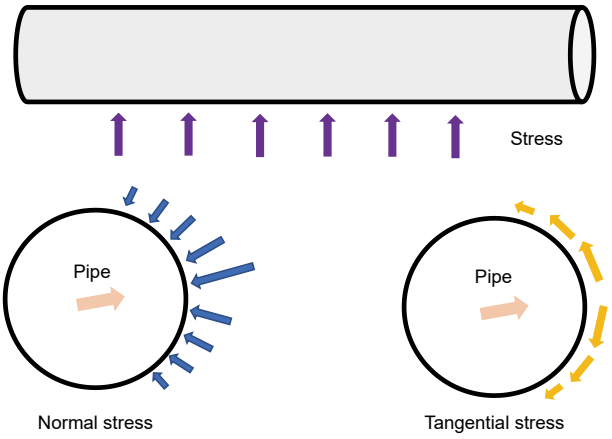

Fig. 14. Schematic representation of stresses acting on pipe surface.

precision of these widely recognized international guidelines for calculating lateral peak soil resistance in pipe-soil interactions.

5. Modified analytical equation and analysis

5.1. Modified results

Studies based on numerical simulations show that the load reduction phase is not pronounced once the burial depth surpasses 2D. The modified soil spring model still employs a bilinear form as characterized in ALA-2001 to maintain conservatism, with adjustments made exclusively to the peak soil resistance. Fig. 21 schematically illustrates these model adjustments.

This study employs multiple linear regression analysis based on 180 sets of FE simulation results encompassing various typical working conditions, including six soil types, five burial depths, and six pipe diameters. By minimizing the residual sum of squares between simulated and predicted values, the model coefficients were optimized to ensure the representativeness of the modified model across the entire parameter space. The peak soil resistance of lateral soil springs was calculated by using Eq. (1) in ALA-2001. Calculations were executed by using Eq. (1) for the scenarios described in Section 4.1 to derive $N_{ch}cD$ and $N_{qh}\bar{\gamma}HD$ as initial independent variables. Based on the analysis of peak soil resistance variation patterns under different influencing factors, transformations were carried out through combinations of initial independent variables and influencing factors, yielding modified independent variable expressions with high goodness-of-fit (R^2). Noteworthy, the formula is based on the equation from the ALA-2001 standard. The formula used in this study is an improved version derived from ALA-2001, with the primary research focusing on determining the regression coefficients for the modified formula. The FE simulation results provide the dependent variable P_u. Regression analysis was performed between the independent and dependent variables to ascertain the regression coefficients. The independent variable outcome improves in the following form: $N_{ch}cD\sqrt{H/D} + N_{qh}\bar{\gamma}HD$. The coefficient of determination (R^2) between the calculations obtained from the modified equation and FE results reaches 0.995, demonstrating high predictive accuracy. The modified equation is described as follows:

$$P_u = 0.83 \times N_{ch}cD\sqrt{H/D} + 0.57 \times N_{qh}\bar{\gamma}HD \quad (6)$$

The peak soil resistance under various operational conditions in Section 4.1 was calculated by using the revised equation. The results from FE simulations act as the reference values (horizontal axis), while the analytical calculation results are plotted for comparative analysis (vertical axis). Fig. 22 depicts error bars of ±10%, ±20%, and ±30%. It indicates that the results derived from the modified equation are more precise, with errors predominantly within ±20%.

5.2. Analysis

This section presents evaluation of the accuracy of the proposed equation by comparing it with experimental results reported by other scholars and conducting applicability analyses under various working conditions.

Liu et al. (2023) conducted pipe-soil interaction tests under different burial depths, using dry natural river sand with no cohesion (soil density = 1746 kg/m^3, internal friction angle = 42.6°). The test pipe was made of unplasticized polyvinyl chloride (φ110 × 5.3 mm, pipe length = 1.6 m) and embedded in sand, with both ends pulled by steel wires, a setup that allowed limited vertical freedom. Table 9 presents comparative analysis between the predicted lateral peak soil resistance from different equations and experimental results reported by Liu et al. (2023). The percentage deviation represents the difference between the

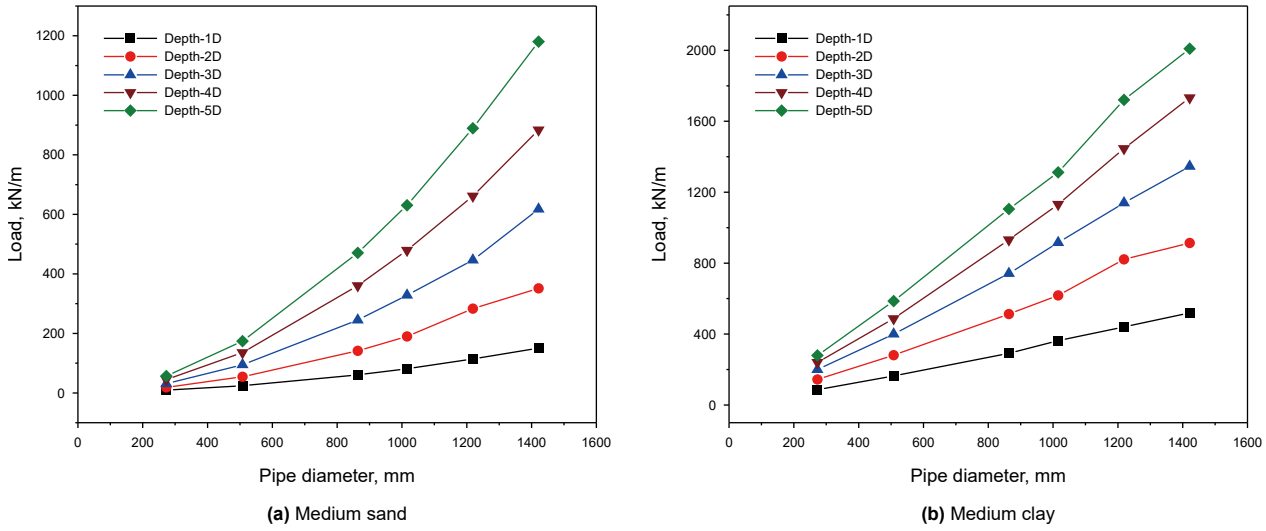

Fig. 15. Comparison of peak soil resistances under different pipe diameters.

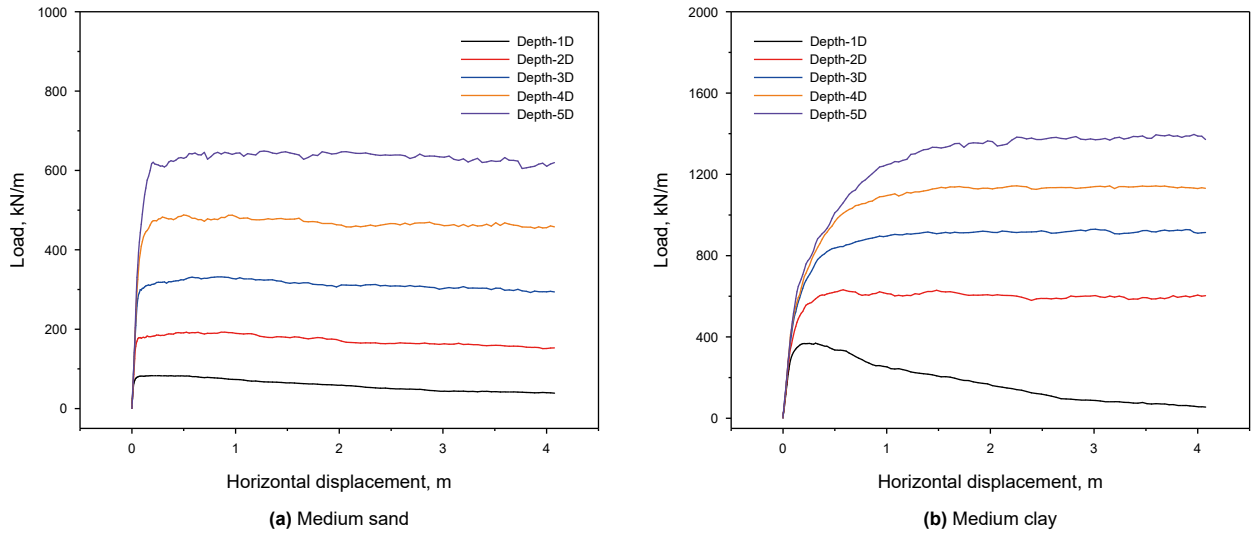

Fig. 16. Load-displacement curves under different burial depths.

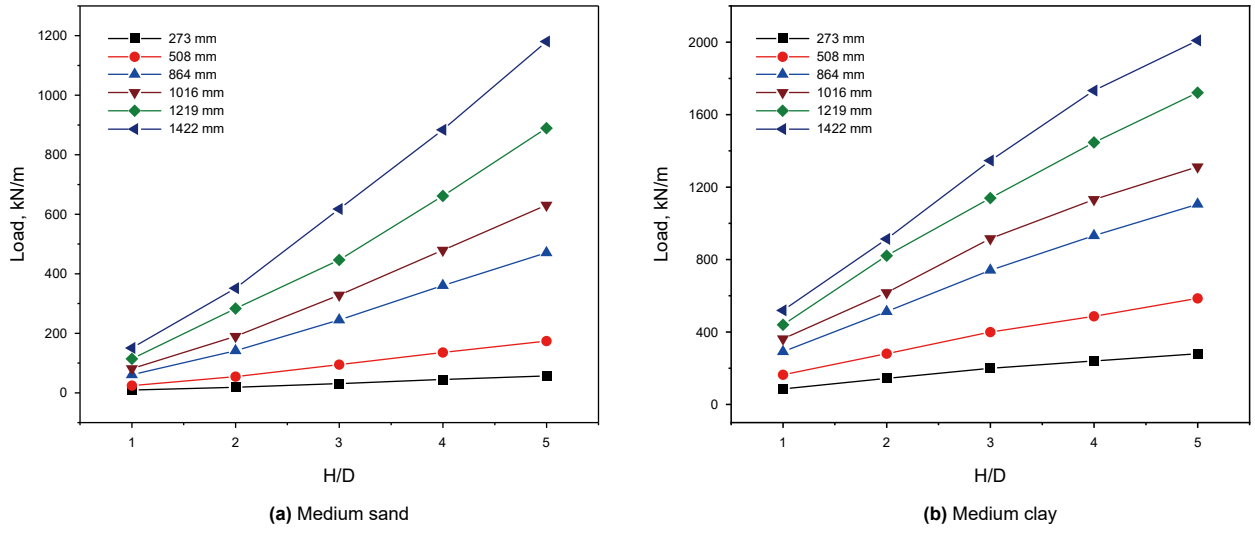

Fig. 17. Comparison of peak soil resistance under different burial depths.

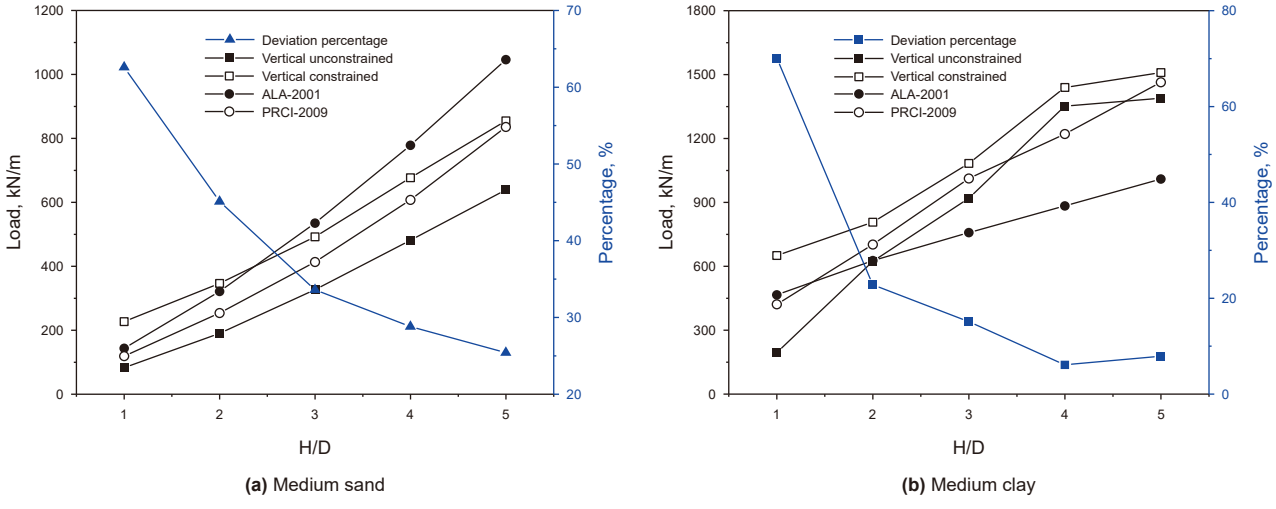

Fig. 18. Peak soil resistance under different vertical constraint conditions.

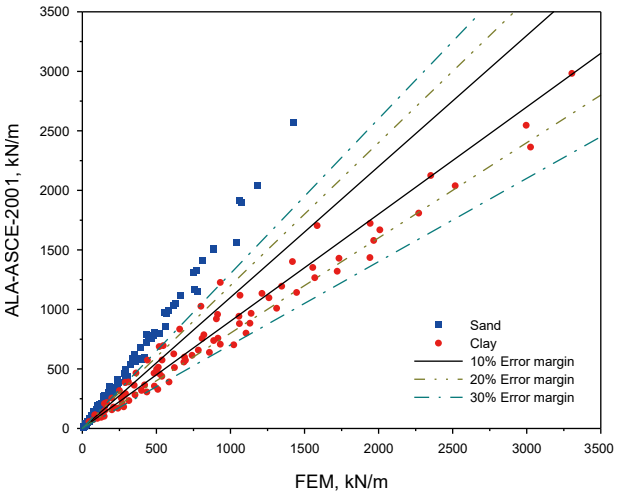

Fig. 19. Comparison of ALA-2001 with FEM.

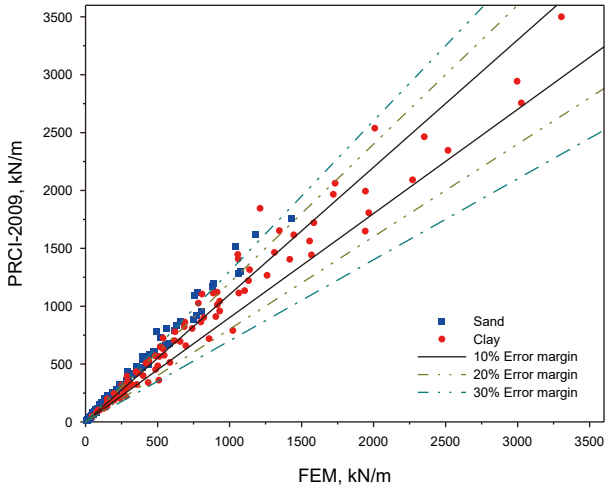

Fig. 20. Comparison of PRCI-2009 with FEM.

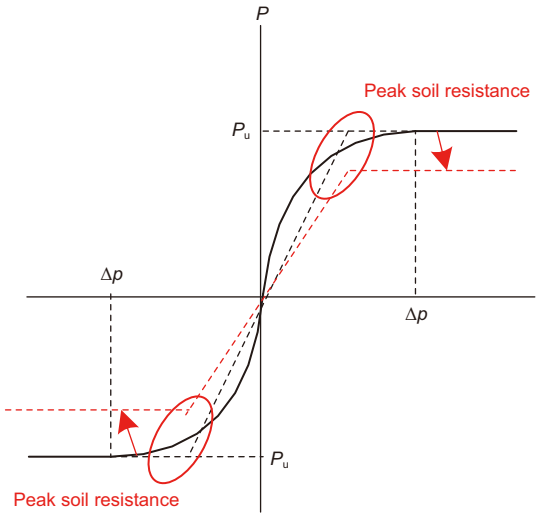

Fig. 21. Schematic illustration of lateral soil spring modification.

calculated results from the equations and the experimental data. The modified equation shows the highest accuracy, with all deviations falling within ±20% of the experimental values. Although PRCI-2009 predictions outperform those of ALA-2001, they remain slightly less accurate than the modified equation.

For comparative analysis of clay soil behavior, experimental data from pipe-soil interaction tests conducted by Liu et al. (2015) were utilized. The investigation employed soft clay from the Bohai Bay region (soil density = 1735 kg/m^3, internal friction angle = 12.4°, cohesion = 6 kPa). The test setup consisted of solid pipes with a centerline burial depth of 2.5D (pipe length = 1.2 m, soil-pipe interaction length = 1 m), where both pipe ends extended beyond the test chamber and were actively pulled by steel rods. The chamber design incorporated sliding grooves with clearances exceeding the pipe diameter. Table 10 presents that the prediction errors of ALA-2001, PRCI-2009 and modified equations increase with increasing pipe diameters. This happens because the minimum pipe diameter in the regression dataset used for the modified equation is 273 mm, which positions the current test diameters (significantly smaller than 273 mm) outside the optimal prediction range. An additional contributing factor is that pipes with smaller diameters exhibit less pronounced upward displacement under lateral loading, which results in greater discrepancies between the predictions from the modified equation and the experimental measurements.

The comparative analysis presented herein involves systematic investigation of lateral peak soil resistances across diverse soil types, burial depths, and pipe diameters to evaluate discrepancies between design methodologies. Table 11 unequivocally demonstrates that cohesive soils exhibit substantially higher peak resistance values than cohesionless soils. This phenomenon can be visually reinforced by the contrasting soil displacement patterns presented in Figs. 15 and 17. Further, comprehensive mechanistic interpretations of this divergence are elaborated in Section 4.2, in particular, the role of soil cohesion and dilation characteristics. Further scrutiny reveals that under conditions of free vertical pipeline restraint, the modified analytical model consistently outperforms both ALA-2001 and PRCI-2009 standards within its validated operational domain. This superiority manifests specifically for medium-shallow burial depths (H/D ≤ 5), conventional pipe diameters (273–1422 mm), and typical soil conditions (sand/clay classifications per Table 7). The enhanced predictive accuracy stems from the incorporation of coupled friction-cohesion effects

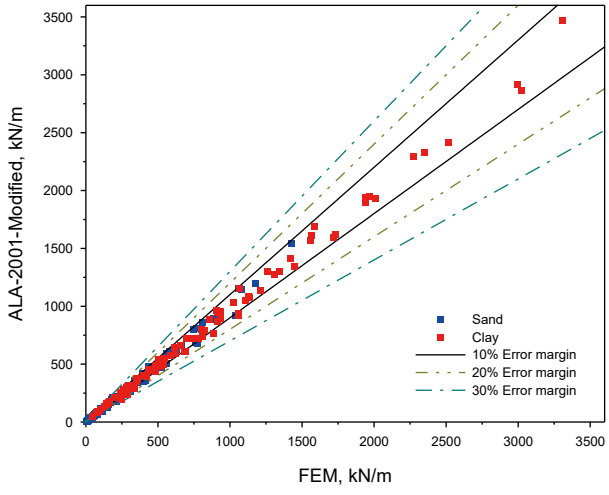

Fig. 22. Comparison of error in results.

Table 9
Comparison between calculated results and experimental data results.

H/D	Experiment, kN/m	ALA-2001, kN/m	Percentage deviation (δ), %	PRCI-2009, kN/m	Percentage deviation (δ), %	Modified equation, kN/m	Percentage deviation (δ), %
2	4.43	8.17	+84.4	4.29	−3.2	4.66	+5.1
5	16.61	28.64	+72.4	15.00	−9.7	16.32	−1.7
8	27.36	57.11	+108.7	30.50	+11.6	32.56	+19.0

Note: The percentage deviation (δ) was calculated as:($\delta = 100\% \times (E_i - T_i)/T_i$), where E_i and T_i represent the calculated result and experimental measurement, respectively.

Table 10
Comparison between calculated results and experimental results.

Pipe diameter, mm	Experiment, kN/m	ALA-2001, kN/m	Percentage deviation (δ), %	PRCI-2009, kN/m	Percentage deviation (δ), %	Modified equation, kN/m	Percentage deviation (δ), %
30	0.90	1.24	+37.7	1.43	+58.9	1.53	+70.0
50	1.50	2.21	+47.3	2.69	+79.3	2.63	+75.3
80	2.12	3.87	+82.5	5.04	+137.7	4.40	+107.5

Note: The percentage deviation (δ) was calculated as:($\delta = 100\% \times (E_i - T_i)/T_i$), where E_i and T_i represent the calculated result and experimental measurement, respectively.

Table 11
Comparison of calculation results obtained by using different equations.

Soil types	H/D	D, mm	FEM, kN/m	ALA-2001, kN/m	Percentage deviation (δ), %	PRCI-2009, kN/m	Percentage deviation (δ), %	Modified, kN/m	Percentage deviation (δ), %
Loose sand	2	1016	159.1	247.5	+55.6	229.3	+44.2	139.0	−12.6
Medium sand			189.6	321.2	+69.4	253.6	+33.8	182.0	−4.0
Dense sand			241.1	475.2	+97.1	312.3	+29.5	275.4	+14.2
Weak clay			349.9	362.1	+3.5	434.4	+24.1	348.9	−0.3
Medium clay			617.3	626.4	+1.5	702.1	+13.7	645.9	+4.6
Stiff clay			1064.8	1118.8	+5.1	1113.6	+4.6	1161.9	+9.1
Medium sand	1	1016	72.6	143.4	+103.1	119.0	+68.6	80.6	+11.0
	2		189.6	321.2	+69.4	253.6	+33.8	182.0	−4.0
	3		328.4	534.8	+62.9	413.4	+25.9	301.3	−8.3
	4		479.3	778.2	+62.4	607.4	+26.7	435.5	−9.1
	5		630.4	1046.3	+66.0	835.5	+32.5	582.2	−7.6
Medium clay	1	1016	362.1	465.4	+28.5	421.4	+16.4	369.8	+2.1
	2		617.3	626.4	+1.5	702.1	+13.7	645.9	+4.6
	3		915.6	757.8	−17.2	1011.9	+10.5	877.2	−4.2
	4		1131.6	883.3	−21.9	1220.9	+7.9	1083.9	−4.2
	5		1311.5	1009.3	−23.0	1464.0	+11.6	1276.2	−2.7
Medium sand	3	273	28.9	42.4	+46.8	36.6	+26.5	23.6	−18.2
		508	94.5	138.6	+46.6	112.5	+19.0	78.2	−17.2
		864	244.5	389.2	+59.2	303.6	+24.2	219.6	−10.2
		1016	328.4	534.8	+62.9	413.4	+25.9	301.3	−8.3
		1219	446.4	765.2	+71.4	586.3	+31.3	430.2	−3.6
		1422	617.4	1036.8	+67.9	789.3	+27.8	581.7	−5.8
Medium clay	3	273	161.5	156.4	−3.2	188.9	+16.9	113.6	−29.6
		508	359.2	318.8	−11.2	400.3	+11.4	297.0	−17.3
		864	720.9	613.8	−14.9	806.8	+11.9	680.2	−5.7
		1016	915.6	757.8	−17.2	1011.9	+10.5	877.2	−4.2
		1219	1139.4	966.8	−15.2	1315.4	+15.4	1168.8	+2.6
		1422	1345.9	1195.0	−11.2	1652.7	+22.8	1491.1	+10.8

Note: The percentage deviation (δ) was calculated as: ($\delta = 100\% \times (E_i - T_i)/T_i$), where E_i and T_i represent the calculated result and experimental result, respectively.

and asymmetric soil constraints in the model, which have been inadequately addressed in existing guidelines.

Notably, for application scenarios extending beyond the calibrated parameter range, including small-diameter pipes (<273 mm), deep burial conditions (H/D > 5), geotechnically complex scenarios (saturated clays, desiccated sands, or shallow embedding in highly deformable strata), and restricted pipeline longitudinal freedom, supplementary validation is required through numerical simulations or physical testing to determine whether to adopt the modified model or current standards. Importantly, for typical working conditions (in particular, within the parameter ranges covered by numerical simulations), the modified model proposed in this study should be preferentially adopted.

6. Conclusions

To address the issue of poor applicability of the existing standards for calculating the lateral peak soil resistance in pipe-soil interaction, relevant research was conducted herein. The testing apparatus for examining pipe-soil interaction was designed, fabricated, and employed to conduct four horizontal tests. A nonlinear finite element model for pipe-soil interaction was established and validated with test results to confirm its precision. Numerical simulations were conducted under various conditions to determine the lateral peak soil resistance. The equation for calculating lateral peak soil resistance in the existing ALA-2001 standard was revised. Several valuable conclusions can be drawn from this research.

(1) A testing apparatus for simulating pipe-soil interaction was designed and constructed. Four tests under varying conditions were conducted using systematic procedures to obtain complete load-displacement curves characterizing pipe-soil interaction, thereby enriching the current experimental database in pipe-soil interaction research. A numerical simulation model for large-displacement pipe-soil interaction was developed via the coupled Eulerian-Lagrangian method in ABAQUS/Explicit. The accuracy of the numerical simulation model was validated against the experimental results from this study, providing a reliable simulation tool for effectively investigating pipe-soil interaction characteristics.

(2) Based on the established finite element numerical simulation model that demonstrates relatively good capability in characterizing pipe-soil interactions under large deformation conditions, peak lateral soil resistance values for various working conditions involving different pipe diameters, burial depths, and soil properties were systematically determined in this study. The effectiveness of the lateral peak soil resistance calculation equations provided in the current standards ALA-2001 and PRCI-2009 was assessed. The significant discrepancies between the two criteria and the simulation results were observed in the calculated lateral peak soil resistance results under various conditions.

(3) A database of lateral peak soil resistance was established, covering various burial depths ($H/D \leq 5$), pipe diameters (273–1422 mm), and typical soil types. Based on this database, a modified equation for lateral peak soil resistance was proposed, and its reliability was further validated through physical test results reported by other researchers. Comparative analysis across multiple working conditions demonstrates that, especially within the parameter range specified in this study, the calculation errors of this modified equation are generally controlled within $\pm 20\%$, with overall accuracy surpassing that of both the ALA-2001 and PRCI-2009 standards. Beyond the parameter range of this study, it is recommended to conduct further validation through numerical simulations or physical tests before deciding whether to adopt this equation.

CRediT authorship contribution statement

Xiao-Ben Liu: Writing – original draft, Project administration, Conceptualization. **Tian-Wei Kong:** Writing – review & editing, Methodology. **Peng-Chao Chen:** Writing – review & editing. **Dong Zhang:** Investigation, Formal analysis. **Wei Huang:** Data curation. **Lei Li:** Resources. **Rui Guo:** Resources.

Declaration of interest Statement

The authors declare that they have no known competing financial interests or personal relationships that could have appeared to influence the work reported in this paper.

Acknowledgements

This research has been co-financed by the Key Science and Technology Project of Ministry of Emergency Management of the People's Republic of China (Grant No. 2024EMST090903), the National Key R&D Program of China (Grant No. 2022YFC3070100), and the Young Elite Scientists Sponsorship Program by Beijing Association for Science and Technology, China (Grant No. BYESS2023261).

References

ALA, 2001. Guidelines for the design of buried steel pipe. American Lifelines Alliance, USA.
Almahakeri, M., Fam, A., Moore, I.D., 2014. Experimental investigation of longitudinal bending of buried steel pipes pulled through dense sand. J. Pipeline Syst. Eng. Pract. 5 (2), 10. https://doi.org/10.1061/(asce)ps.1949-1204.0000141.
Ansari, Y., Kouretzis, G., Sloan, S.W., 2021. Physical modelling of lateral sand-pipe interaction. Geotechnique 71 (1), 60–75. https://doi.org/10.1680/jgeot.18.P.119.
ASCE, 1984. Guidelines for the seismic design of oil and gas pipeline systems. American Society of Civil Engineers, USA. https://doi.org/10.1115/IPC2002-27330.
Audibert, J., Nyman, K., 1977. Soil restraint against horizontal motion of pipes. J. Geotech. Eng. Div. 103 (10), 1119–1142.
C-CORE, 2003. Extended model for pipe soil interaction. R-02-044–113. Pipeline Research Council International.
Fei, K., Zhang, J., 2013. Application of ABAQUS in geotechnical engineering. China Water & Power Press, Beijing, China (in Chinese).
Guo, P.J., Stolle, D.F., 2005. Lateral pipe–soil interaction in sand with reference to scale effect. J. Geotech. Geoenviron. Eng. 131 (3), 338–349. https://doi.org/10.1061/(ASCE)1090-0241(2006)132:10(1372.
Hansen, J., Brinch, J., 1961. The ultimate resistance of rigid piles against transversal forces. Dan. Geotech. 12, 1–9.
Hsu, T.W., 1996. Soil restraint against oblique motion of pipelines in sand. Can. Geotech. J. 33 (1), 180–188. https://doi.org/10.1139/t96-034.
Hsu, T.W., Chen, Y.J., Wu, C.Y., 2001. Soil friction restraint of oblique pipelines in loose sand. J. Transport. Eng. 127 (1), 82–87. https://doi.org/10.1061/(ASCE)0733-947X(2001)127:1(82.
Hsu, T.W., Chen, Y.J., Hung, W.C., 2006. Soil restraint to oblique movement of buried pipes in dense sand. J. Transport. Eng. 132 (2), 175–181. https://doi.org/10.1061/(ASCE)0733-947X(2006)132:2(175.
Hua, J., Zheng, J., 2018. Geological engineering handbook. China Architecture & Building Press, Beijing, China (in Chinese).
Karimian, S.A., 2006. Response of buried steel pipelines subjected to longitudinal and transverse ground movement. The University of British Columbia (Canada), British Columbia, Canada.
Ko, J., Jeong, S., Lee, J.K., 2016. Large deformation FE analysis of driven steel pipe piles with soil plugging. Comput. Geotech. 71, 82–97. https://doi.org/10.1016/j.compgeo.2015.08.005.
Kouretzis, G.P., Sheng, D.C., Sloan, S.W., 2013. Sand-pipeline-trench lateral interaction effects for shallow buried pipelines. Comput. Geotech. 54, 53–59. https://doi.org/10.1016/j.compgeo.2013.05.008.
Liang, Y.T., Tu, R.F., Zhang, H., et al., 2025. Role of oil and gas pipelines in the construction of a new energy system with multi-energy integration. Oil Gas Storage Transp. 44 (4), 361–378 (in Chinese).
Liu, J.Q., Xie, Q.W., Ye, M.G., et al., 2023. Response of UPVC pipes buried in sand under lateral ground movement. Tunn. Undergr. Space Technol. 138, 14. https://doi.org/10.1016/j.tust.2023.105177.
Liu, R., Guo, S.Z., Yan, S.W., 2015. Study on the lateral soil resistance acting on the buried pipeline. J. Coast Res. 391–398. https://doi.org/10.2112/si73-069.1.
Liu, W.H., Wei, Z.K., Xiao, L., et al., 2019. Experimental analysis of soil compactness on erosion intensity of bare soil. Science of Soil and Water Conservation 17 (6), 52–60.
MIIT, 2017. Series of steel pipe size in petrochemical industry, SH/T 3405. China Petrochemical Press, China (in Chinese).
MOHURD, 2017. Seismic technical code for oil and gas transmission pipeline engineering, GB/T 50470. China Planning Press, China (in Chinese).
MOHURD, 2019. Standard for geotechnical testing method, GB/T 50123. China Planning Press, China (in Chinese).
Ovesen, N.K., Bulletin, J., 1964. Anchor slabs, calculation methods and model tests, vol. 16, p. 39.
PRCI, 2009. Guidelines for constructing natural gas and liquid hydrocarbon pipelines through areas. PRCI, USA.
Sarvanis, G.C., Karamanos, S.A., Vazouras, P., et al., 2018. Permanent earthquake-induced actions in buried pipelines: Numerical modeling and experimental verification. Earthq. Eng. Struct. Dynam. 47 (4), 966–987. https://doi.org/10.1002/eqe.3001.
Spyros, A., 2021. Geohazards and pipelines. Springer Nature Switzerland AG, Cham, Switzerland.
Trautmann, C.H., O'Rourke, T.D., 1985. Lateral force-displacement response of buried pipe. J. Geotech. Eng. Div. 111 (9), 1077–1092. https://doi.org/10.1061/(ASCE)0733-9410(1985)111:9(1077.
Wantland, G.M., O'Neill, M.W., Kalajian, E.H., et al., 1982. Pipeline lateral stability in soft clay. J. Petrol. Technol. 34 (1), 217–220. https://doi.org/10.2118/8528-PA.
Wu, J.B., Kouretzis, G., Suwal, L., et al., 2020. Shallow and deep failure mechanisms during uplift and lateral dragging of buried pipes in sand. Can. Geotech. J. 57 (10), 1472–1483. https://doi.org/10.1139/cgj-2019-0281.
Yimsiri, S., Soga, K., Yoshizaki, K., et al., 2004. Lateral and upward soil-pipeline interactions in sand for deep embedment conditions. J. Geotech. Geoenviron. Eng. 130 (8), 830–842. https://doi.org/10.1061/(ASCE)1090-0241(2004)130:8(830.
Yue, H.Y., Zhuang, P.Z., Song, X.G., et al., 2021. Soil restraint on buried pipelines during oblique relative movements in sand. Mar. Georesour. Geotechnol. 39 (12), 1505–1515. https://doi.org/10.1080/1064119x.2020.1849472.
Zhang, H.D., 2024. Analysis of pipeline stress state and risk assessment under slope conditions. China University of Mining and Technology. Master Thesis.